$MgSiO_3$ postperovskite at D″ conditions

Renata M. Wentzcovitch*, Taku Tsuchiya†, and Jun Tsuchiya†

Department of Chemical Engineering and Materials Science, Minnesota Supercomputing Institute for Digital Technology and Advanced Computation, University of Minnesota, 421 Washington Avenue Southeast, Minneapolis, MN 55455

Edited by Ho-kwang Mao, Carnegie Institution of Washington, Washington, DC, and approved November 14, 2005 (received for review August 9, 2005)

The postperovskite transition in $MgSiO_3$ at conditions similar to those expected at the D″ discontinuity of Earth's lower mantle offers a paradigm for interpreting the properties of this region. Despite consistent experimental and theoretical predictions of this phase transformation, the complexity of the D″ region raises questions about its geophysical significance. Here we report the thermoelastic properties of *Cmcm* postperovskite at appropriate conditions and evidences of its presence in the lowermost mantle. These are (*i*) the jumps in shear and longitudinal velocities similar to those observed in certain places of the D″ discontinuity and (*ii*) the anticorrelation between shear and bulk velocity anomalies as detected within the D″ region. In addition, the increase in shear modulus across the phase transition provides a possible explanation for the reported discrepancy between the calculated shear modulus of postperovskite free aggregates and the seismological counterpart in the lowermost mantle.

Earth's mantle | elasticity | D″ layer | core–mantle boundary

The recent discovery of the postperovskite transition in $MgSiO_3$ (1) was followed by a series of new findings that may shed light on the enigmatic properties of the D″ layer, the lowest 250 km of Earth's lower mantle (LM), just above the core–mantle boundary. Pressures in this region vary from ≈125 to ≈135 GPa, while temperatures should vary from ≈2,500 to ≈4,000 K. So far, two first-principles quasiharmonic calculations (2, 3) have offered consistent thermodynamic phase boundaries compatible with experimental findings (1, 3–6) and with seismologic/geodynamic inferences of this region (7). Static first principles elasticity calculations (3, 8–10) have indicated that postperovskite's elasticity may cause some of the puzzling observations of this region, such as discontinuity jumps, anisotropy, and lateral heterogeneities. Because of the static nature of these calculations, these inferences were not definite.

Here we present the thermoelastic properties of the postperovskite phase at relevant conditions obtained by first-principles computations within the quasiharmonic approximation. We compute shear, longitudinal, and bulk velocities of the postperovskite phase, compare with those of the perovskite phase (11), and, by invoking our previous thermodynamic phase boundary (2), we predict the seismic signature of its presence in the LM, i.e., density and velocity jumps across this transformation. We also predict in a continuum P,T space various ratios of relative changes in velocities and density caused by temperature and phase change in pure aggregates. They prove to be fundamental for interpreting the unexplained origin of lateral heterogeneities in D″.

Results and Discussion

The elastic constants of $MgSiO_3$ postperovskite are remarkably different from those of perovskite (11). Postperovskite is a layered structure, expands anisotropically, and has complex pressure- and temperature-dependent elastic behavior (see ref. 8 and Fig. 4, which is published as supporting information on the PNAS web site). However, its aggregate moduli do not differ dramatically from those of perovskite. The adiabatic bulk moduli of both phases, $B_S(P, T)$ (Fig. 1*A*), are very similar at >80 GPa. The shear modulus of postperovskite, $G(P, T)$ (Fig. 1*A*), is larger and has larger pressure and temperature gradients. This result and the fact that postperovskite is ≈1.5% denser than perovskite at deep LM conditions determine the velocity contrasts between these phases. The shear velocity, $V_S(P, T)$, of postperovskite and its gradients are larger than those of perovskite (see Fig. 1 legend and ref. 11). Because of $G(P, T)$, postperovskite's $V_S(P, T)$ is also larger and has larger gradients. The longitudinal velocity, $V_P(P, T)$, is a little larger and has slightly larger gradients because of $G(P, T)$ as well (see Fig. 1*B*). In contrast, the bulk velocity, $V_\phi(P, T)$, is smaller than that of perovskite because of their similar $B_S(P, T)$ values and the larger density (ρ) of postperovskite. Something similar is observed across the phase transition in postperovskite synthesized from natural samples of $(Mg,Fe)SiO_3$ orthopyroxene (14). Fig. 1*C* shows the velocity jumps across the calculated phase boundary (2) (see Fig. 1 legend). These results are consistent with the increase in seismic velocities observed ≈200–300 km above the core–mantle boundary in certain places (15) but most easily detected beneath regions of past subduction, presumably cold places, such as beneath Central America (15). There, $\Delta V_S > \Delta V_P$ and $\Delta V_S \approx$ 2–3% is observed, but this observation is clearly a regional property of a notably heterogeneous layer (refs. 16–18 and references therein).

Another baffling property of D″ revealed by global tomographic models (19) is the anticorrelation between lateral (isobaric) heterogeneities in V_ϕ and V_S. The likely causes are usually addressed by comparing the seismic parameters, $R_{S/P} = (\partial \ln V_S/\partial \ln V_P)_P$ and $R_{\phi/S} = (\partial \ln V_\phi/\partial \ln V_S)_P$, to theoretical or experimental predictions of these ratios at relevant conditions (20). It is known that in the shallow LM $R_{S/P} \sim 2.3$ and $R_{\phi/S} \sim 0.0$, whereas in D″ $R_{S/P} \sim 3.4$ and $R_{\phi/S} \sim -0.2$ (19). Velocity anomaly ratios produced by isobaric temperature changes in pure postperovskite and perovskite aggregates are displayed in Fig. 2 *A* and *B* along with the seismic parameters extracted from ref. 19 and reported in ref. 20. In pure perovskite aggregates, $R_{S/P}$ increases with pressure and temperature but reaches at most ≈2.3 at 135 GPa and 4,000 K, whereas $R_{\phi/S}$ is approximately pressure independent and slightly decreases with temperature to reach ≈0.16 at similar *P*, *T* values (see Fig. 2*A*). In postperovskite $R_{S/P}$ decreases with pressure, but because of its larger $(\partial G/\partial T)_P$, it increases more rapidly with temperature to reach ≈ 2.8 at the same *P*, *T* values. $R_{\phi/S}$ is smaller than that of perovskite, 0.1, at these conditions (see Fig. 2*B*). It has been argued that anelasticity, anisotropy effects, and lateral variations in calcium content in the deepest mantle might be necessary to produce large values for $R_{S/P}$ and negative ones for $R_{\phi/S}$, unless there is a phase transformation (20).

Fig. 2*C* compares the seismic parameters with the computed ratios of velocity anomalies caused by the postperovskite transition along our phase boundary (2). Very large values for $R_{S/P}$ (>6) and negative values for $R_{\phi/S}$ (<−0.5) result from this phase change. Therefore, lateral variation in phase abundances en-

---

Conflict of interest statement: No conflicts declared.

This paper was submitted directly (Track II) to the PNAS office.

Abbreviations: LM, lower mantle; PREM, Preliminary Reference Earth Model.

*To whom correspondence should be addressed. E-mail: wentzcov@cems.umn.edu.

†Present address: Geodynamics Research Center, Ehime University, Bunkyo-cho 2-5, Matsuyama 790-8577, Japan.

© 2006 by The National Academy of Sciences of the USA

www.pnas.org/cgi/doi/10.1073/pnas.0506879103

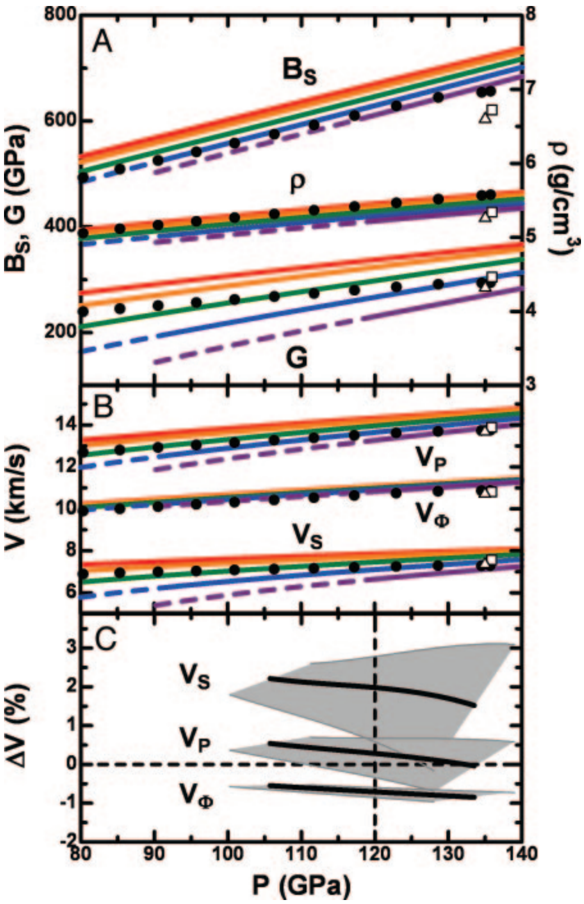

Fig. 1. Elastic properties as functions of pressure and temperature. (*A*) Pressure dependence of aggregate adiabatic bulk (B_S) and shear (G) moduli and density (ρ) of postperovskite along the 300 K (red), 1,000 K (orange), 2,000 K (green), 3,000 K (blue), and 4,000 K (purple) isotherms. (*B*) Isotropic longitudinal [$V_P = \sqrt{(B_S + 4G/3)/\rho}$], shear ($V_S = \sqrt{G/\rho}$), and bulk ($V_S = \sqrt{B/\rho}$) wave velocities. Filled circles in *A* and *B* are PREM values (12) for comparison. (*C*) Velocity jumps across the previously obtained phase boundary (2). Thick black lines represent the jumps at the center of our phase boundary with a density functional theory-related uncertainty of 10 GPa. Shaded areas are possible values throughout the boundary uncertainty domain (2). Open triangles and squares, respectively, are results from molecular dynamics simulations at 135 GPa and 4,000 K and 136 GPa and 3,000 K (13).[‡] The vertical dashed line indicates the approximate topmost location of the D″ discontinuity.

hances the seismic parameters in the correct directions. This effect was approximately estimated in ref. 3 assuming the temperature dependence of perovskite and postperovskite's velocities were the same. The presence of secondary phases, such as magnesiowüstite and $CaSiO_3$, will decrease these anomaly ratios. In addition, the phase boundary and the velocities of minor element bearing perovskite and postperovskite should produce a P, T domain for perovskite/postperovskite coexistence also with unknown properties. Nevertheless, the effect of lateral variations of phase abundances on these parameters seems very robust.

As pointed out from the outset, the topography of D″ is consistent with a phase transition with positive Clapeyron slope ($\approx$4–10 MPa·K^{-1}) induced by lateral temperature variations (7). Interestingly, the correlation between geographic location and

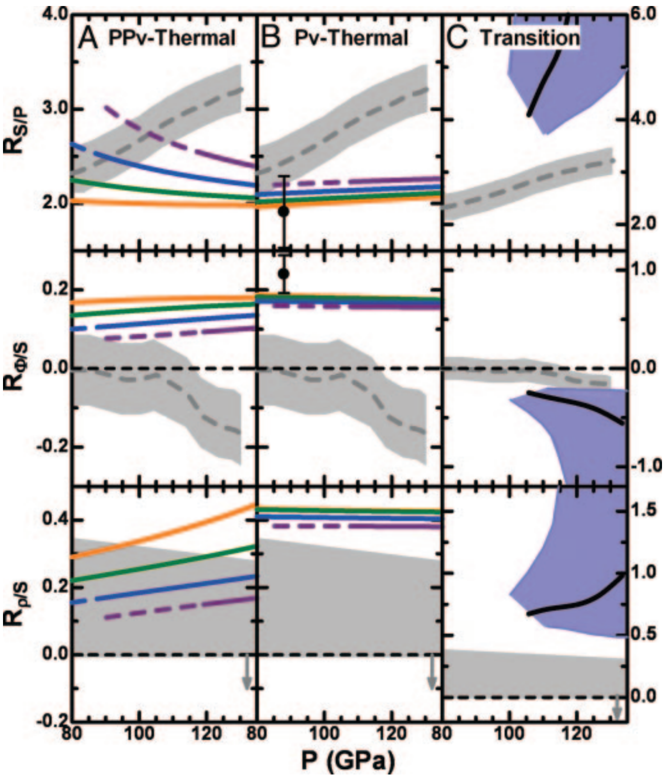

Fig. 2. Ratios of velocities and/or density anomalies. Seismic parameters $R_{S/P} = (\partial \ln V_S/\partial \ln V_P)_P$, $R_{\phi/S} = (\partial \ln V_\phi/\partial \ln V_P)_P$, and $R_{\rho/S} = (\partial \ln \rho/\partial \ln V_S)_P$ at several temperatures for postperovskite (*A*) and perovskite (*B*) (color code same as in Fig. 1). These values are presented for comparison. Filled circles with error bar (±20%) are from molecular dynamics simulations (13). (*C*) Contribution of phase transition to these parameters with uncertainties (shaded blue areas) related to phase boundary computation (same as in Fig. 1*C*). Seismic values extracted from ref. 19 and uncertainties (gray shaded areas) were summarized in ref. 20.

nature of V_ϕ and V_S anomalies is also consistent with this assumption if postperovskite is abundant in D″. Beneath the Central Pacific V_ϕ is faster and V_S is slower than their spherical mantle averages, whereas beneath the Circum-Pacific the opposite holds. These regions are generally considered to be respectively hotter and colder than average. The positive Clapeyron slope of this transition implies that hotter regions should contain less postperovskite and therefore have faster V_ϕ and slower V_S, whereas colder regions should be enriched in the latter and have slower V_ϕ and faster V_S, as observed. Lateral variations in phase abundances alone do not account for the complex structure and properties of D″. However, this perspective should be useful as a reference model from which deviations should be interpreted. Obviously the effect of secondary phases and minor element partitioning on the postperovskite phase boundary and on aggregate elasticity, particularly the important effect of iron (21), must be determined before a more quantitative reference mineralogical model for D″ is developed.

The origin of the negative values of $R_{\phi/S}$ above D″ indicated in Fig. 2*B* is also unclear. It could originate in the degree of resolution of tomographic models. However, if this effect is real, it could have several origins, including anelasticity. A possible mineralogical origin and an argument against anelasticity alone will be discussed at the end of the text in connection with the elasticity of postperovskite-free aggregates (11) and the stability of iron-rich postperovskite (21).

These results and inferences imply that a third seismic parameter, $R_{\rho/S} = (\partial \ln \rho/\partial \ln V_S)_P$, the average ratio between ρ and V_S

[‡] The molecular dynamics simulation in ref. 13 used a supercell of 60 atoms and the GGA approximation for exchange correlation. The latter is the likely source of the discrepancy in B_S, the adiabatic bulk modulus, displayed in Fig. 1.

anomalies caused by the postperovskite transition, should be positive and perhaps increase with depth in the lowermost mantle (see lowest portion of Fig. 2*C*), unless other effects such as change in anelastic effects or chemical heterogeneities (18, 20, 22)[§] occur simultaneously. Some 3D density models do not support this prediction (24), whereas others do (25). Estimates of this parameter obtained by joint inversions of seismic and geodynamic data also tend to offer a positive ratio (26). It appears that until a clear consensus on the 3D structure of ρ is reached, this issue will remain an open point. Recently, it has been pointed out that an average excess density of 0.4% in the lowermost mantle is possible (27), in agreement with our expectations.

Another pressing issue is the anisotropy of D″, a case of boundary layer anisotropy possibly enhanced by the bias of seismic detection techniques toward these regions. Despite the lack of global seismic coverage of D″, the observed diversity of anisotropy styles (16, 28), and the numerous possible sources of anisotropy (29), evidence has been accumulating suggesting that anisotropy in certain places of D″ could result from lattice preferred orientation in largely strained aggregates produced by mantle circulation (ref. 30 and references therein). The analogy between the D″ region and the topmost upper mantle, where anisotropy is also strong, is very compelling. Beneath regions of past and present subduction, such as the Caribbean, where colder than average and largely deformed paleo-plates are expected to reside, and horizontal flow presumably happens, transverse isotropy with $V_{\mathrm{SH}} > V_{\mathrm{SV}}$ is generally observed [$V_{\mathrm{SH(SV)}}$ being the velocity of horizontally (vertically) polarized shear waves propagating horizontally]. It is plausible that in postperovskite the primary slip system involves (010). Lateral material displacement should then align mainly the silica layers parallel to the horizontal plane. However, this simple picture does not provide a satisfactory explanation for the anisotropy in D″ (8). Static elasticity calculations have shown that ($V_{\mathrm{SH}} - V_{\mathrm{SV}}$) in transversely isotropic aggregates with this preferred orientation is positive but small (2, 3, 8). The largest V_{S} splitting is produced by aligning [001] vertically, not [010] (8).

Fig. 3 shows the calculated shear wave splittings along the thermodynamic phase boundary (2) for various vertical alignments of the crystalline axes of these phases and of periclase (MgO) (31),[¶] the presumably most abundant secondary phase in the LM. It can be seen that at relevant *P*, *T* conditions that (*i*) vertical alignment of postperovskite's [001] produces the largest positive ($V_{\mathrm{SH}} - V_{\mathrm{SV}}$) but considerably smaller than that predicted at $T = 0$ K (8); (*ii*) the shear wave splittings in perovskite and postperovskite have similar magnitudes regardless of orientation; (*iii*) similarly to the static results (32), only vertical alignment of perovskite's [100] produces positive ($V_{\mathrm{SH}} - V_{\mathrm{SV}}$); and (*iv*) horizontal alignment of MgO's {100}, its primary slip plane at high *P*s (33), produces considerably larger ($V_{\mathrm{SH}} - V_{\mathrm{SV}}$). Despite our lack of direct information on the slip systems of these phases at D″ conditions, it appears that unless a significant alteration in plastic deformation mechanism from diffusion to dislocation creep accompanies the postperovskite transition, it is unlikely that postperovskite can be a more significant source of anisotropy in D″ than perovskite.

Despite being less abundant (≈20 vol%) magnesiowüstite (33) is the most anisotropic (31, 34) and weaker phase present. It is therefore likely to undergo more extensive deformation (33) and be a more important source of lattice preferred orientation-derived anisotropy (30), particularly in D″. Across the postperovskite transition, the contrast in strength between $\mathrm{MgSiO_3}$ and MgO should increase because the strength of a material usually increases with the shear modulus (see Table 1). MgO therefore could undergo greater deformation next to postperovskite.

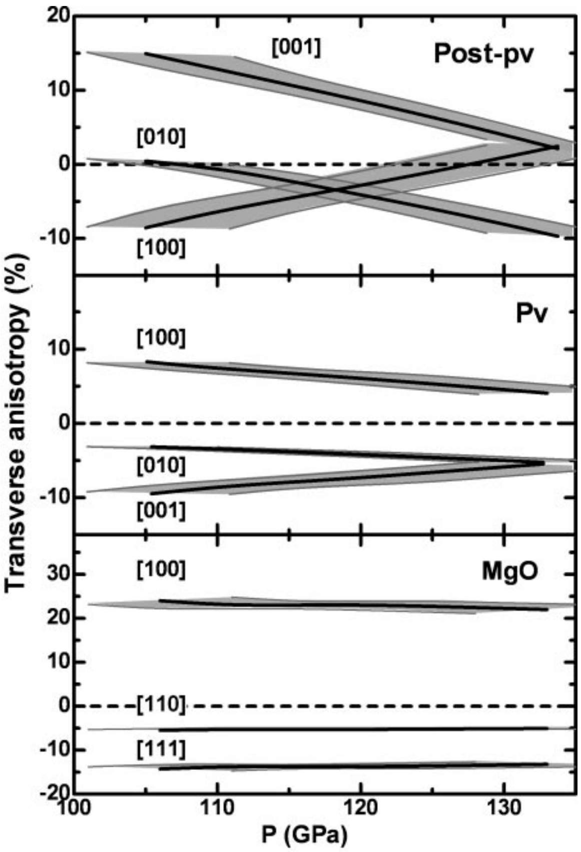

Fig. 3. Shear wave splittings ($V_{\mathrm{SH}} - V_{\mathrm{SV}}$) (see text) in $\mathrm{MgSiO_3}$ postperovskite and perovskite, along the thermodynamic phase boundary with respective uncertainties, for horizontally propagating waves in transversely isotropic aggregates with three possible alignments of the major crystalline axes along the vertical direction.

Finally, it has been pointed out (11) that *G* in the shallow LM, as extracted from the Preliminary Reference Earth Model (PREM; G^{PREM}) (12), agrees well with that of an aggregate of (Mg,Fe)$\mathrm{SiO_3}$-perovskite and (Mg,Fe)O with approximately pyrolitic composition at *T*s predicted by a standard adiabatic geotherm (G^{calc}) (35). However, in the deep LM G^{PREM} exceeds G^{calc} by ≈10–15 GPa, i.e., differs by more than estimated uncertainties (11). The nonthermal nature of this phenomenon was indicated by the reasonably good agreement between $B_{\mathrm{S}}^{\mathrm{PREM}}$ and $B_{\mathrm{S}}^{\mathrm{calc}}$, or possibly a slightly smaller $BB_{\mathrm{S}}^{\mathrm{PREM}}$. Presently, the larger G^{PREM} is an argument against anelasticity in the LM. PREM, being a 1D model with a narrow D″ layer only 150-km thick without discontinuities in this region, smoothes the effect of a discontinuous increase in V_{S} and *G* throughout the lowermost mantle (ref. 16 and references therein). Therefore, the existence of postperovskite with larger *G* (≈20 GPa; see Table 1) in the D″ layer could contribute to the type of inconsistency between G^{PREM} and G^{calc} observed in ref. 11.

Another enticing origin for this inconsistency could be of mineralogical nature. With respect to a homogeneous and postperovskite free LM, the existence of a nonhomogeneous distribution of postperovskite introduces positive shear and negative bulk velocity heterogeneities. Their spherical averages increase and decrease as well. The spherically averaged shear

---

[§] Ref. 22 indicates the existence of excess iron in the mantle beneath Hawaii, presumably originating at the core–mantle boundary. This chemical heterogeneity should result in negative $R_{\rho/S}$ (23) as appears to be observed (24).

[¶] The high *P*, *T* elasticity of MgO was presented in ref. 31.

Table 1. Elastic properties in GPa, km/s, and K of $MgSiO_3$ perovskite (1) and postperovskite (2, 4, 6) at 125 GPa and 2,500 K and (3) 140 GPa and 4,000 K

Property	c_{11}	c_{22}	c_{33}	c_{12}	c_{13}	c_{23}	c_{44}	c_{55}	c_{66}	B_S	G	V_P	V_S	V_Φ
(1) M	874	1095	1077	539	436	469	311	255	296	655	276	13.9	7.2	11.1
(2) M	1146	888	1139	454	418	507	311	238	352	656	294	14.0	7.4	11.1
(3) M	1119	900	1131	498	486	536	343	231	326	685	284	14.0	7.3	11.3
(4) $\partial M/\partial P$	6.4	4.5	6.3	2.9	2.3	2.5	3.1	2.2	2.7	3.6	2.2	0.032	0.022	0.022
(5) $\partial M/\partial T$	−0.083	−0.037	−0.069	0.0011	0.022	−0.0054	−0.011	−0.028	−0.045	−0.017	−0.030	−0.00029	−0.0003	−0.000073
(6) $\partial^2 M/\partial P \partial T$	0.00061	0.00017	0.00026	−0.000063	0.000089	−0.00013	0.00076	0.00030	0.00014	0.000063	0.00032	0.0000035	0.0000053	0.0000012

Diagonal c_{ij}s are typically underestimated by ≈2%, off-diagonal ones by ≈1.5%, and shear ones by <1%. B_S and G are Voigt–Reuss–Hill averaged adiabatic bulk and shear moduli. Typically they are underestimated by 2% (random deviations in individual c_{ij} are averaged out). V_P, V_S, and V_Φ are compressional, shear, and bulk velocities.

and bulk moduli increase and remain approximately unchanged (or decrease slightly depending on the average geotherm), respectively. Ref. 11 pointed to this type of deviation starting at pressures as low as ≈75 GPa. This finding and the simultaneous observation of anticorrelations above ≈80 GPa indicated in Fig. 2 could be pointing to the existence of postperovskite already at these pressures, perhaps in regions with substantially greater iron content (20), or of another phase introducing the same type of elastic anomaly. In short, the origin of negative $R_{\phi/S}$ values above D″ could be the same as of those discrepancies observed in ref. 11.

This discussion is speculative, but it is essential to recognize this relationship. Until we have more information about equilibrium high *P*, *T* properties of (low and high spin) iron bearing aggregates this issue will not be simply tackled, including the role of anelasticity.

Theoretical Methods

The methodology used here has been used in several previous investigations and reported in detail in other publications (2, 9, 11, 36) and is described in *Supporting Methods*, which is published as supporting information on the PNAS web site, with individual elastic constants of postperovskite and perovskite. It proved very successful when applied to the perovskite phase (11) at these conditions, producing results in excellent agreement with those obtained in molecular dynamics calculations (37). A recent investigation of the thermodynamic properties of the postperovskite phase (36) indicates that the quasiharmonic approximation is also valid for this phase at relevant conditions. Both phases are mechanically and vibrationally very stable well beyond their thermodynamic stability fields, and, at D″ conditions, their thermodynamic properties are very similar (36). This characteristic is reflected in the nature of the postperovskite transformation: it is kinetically slow displaying large hysteresis in pressure (1, 4, 5).

We thank Koichiro Umemoto for assistance with earlier calculations and Don Weidner and participants of the Cooperative Institute for Deep Earth Research workshop (National Science Foundation Grants PHY99-0794 and EAR-0215587) where these results were first presented for helpful discussions. This work was supported by National Science Foundation Grants EAR-0135533, EAR-0230319, and ITR-0428774. J.T. and T.T. were supported in part by the Japan Society for the Promotion of Science (JSPS).

1. Murakami, M., Hirose, K., Kawamura, K., Sata, N. & Ohishi, Y. (2004) *Science* **304,** 855–858.
2. Tsuchiya, T., Tsuchiya, J., Umemoro, K. & Wentzcovitch, R. M. (2004) *Earth Planet. Sci. Lett.* **224,** 241–248.
3. Oganov, A. R. & Ono, S. (2004) *Nature* **430,** 445–448.
4. Shim, D., Duffy, T. & Jeanloz, R. (2004) *Geophys. Res. Lett.* **31,** L10603.
5. Mao, W. L., Shen, G., Prakapenka, V. B., Meng, Y., Campbell, A. L., Heinz, D. L., Shu, J., Hemley, R. J. & Mao, H. K. (2004) *Proc. Natl. Acad. Sci. USA* **101,** 15867–15869.
6. Ono, S. & Oganov, A. (2005) *Earth Planet. Sci. Lett.* **236,** 914–932.
7. Sidorin, I., Gurnis, M. & Helmberger, D. (2004) *Science* **286,** 1326–1331.
8. Tsuchiya, T., Tsuchiya, J., Umemoto, K. & Wentzcovitch, R. M. (2004) *Geophys. Res. Lett.* **31,** L14603.
9. Iitaka, T., Hirose, K., Kawamura, K. & Murakami, M. (2004) *Nature* **430,** 442–445.
10. Caracas, R. & Cohen, R. E. (2005) *Geophys. Res. Lett.* **32,** L16310.
11. Wentzcovitch, R. M., Karki, B. B., Cococcioni, M. & de Gironcoli, S. (2004) *Phys. Rev. Lett.* **92,** 01801.
12. Dziewonski, A. D. & Anderson, D. L. (1981) *Phys. Earth Planet. Int.* **25,** 297–356.
13. S. Stackhouse, S., Brodholt, J. P., Wookey, J., Kendall, J.-M. & Price, G. D. (2005) *Earth Planet. Sci. Lett.* **230,** 1–10.
14. Shieh, S. R., Duffy, T. S., Kubo, A., Shen, G., Prakapenka, V. B., Sata, N., Hirose, K. & Ohishi, U. (2006) *Proc. Natl. Acad. Sci. USA*, in press.
15. Lay, T. & Helmberger, D. V. (1983) *Geophys. J. R. Astron. Soc.* **75,** 799–838.
16. Wysession, M. E., Lay, T., Revenaugh, J., Williams, Q., Garnero, E. J., Jeanloz, R. & Kellogg, L. H. (1998) in *Core-Mantle Boundary Region*, Geodynamics Series, eds. Gurnis, M., Wysession, M. E., Knittle, E. & Buffet, B. (Am. Geophys. Union, Washington, DC), Vol. 28, pp. 273–297.
17. Garnero, E. (2004) *Science* **304,** 834–836.
18. Lay, T., Garnero, E. J. & Williams, Q. E. (2004) *Phys. Earth Planet. Int.* **146,** 441–467.
19. Masters, G., Laske, G., Bolton, H. & Dziewonski, A. (2000) *Earth's Deep Interior: From Mineral Physics and Tomography from Atomic to the Global Scale*, Geophysical Monograph Series, eds. Karato, S., Forte, A. M., Liebermann, R. C., Masters, G. & Stixrude, L. (Am. Geophys. Union, Washington, DC), Vol. 117, p. 63–87.
20. Karato, S. & Karki, B. B. (2001) *J. Geophys. Res.* **106,** B21771–B21783.
21. Mao, W. L., Meng, Y., Shen, G., Prakapenka, V. B., Campbell, A. J., Heinz, D. L., Shu, J., Caracas, R., Cohen, R. E., Fei, Y., *et al.* (2005) *Proc. Natl. Acad. Sci. USA* **102,** 9751–9753.
22. Humayun, M., Qin, L. & Norman, M. D. (2004) *Science* **306,** 91–94.
23. Kiefer, B., Stixrude, L. & Wentzcovitch, R. M. (2002) *Geophys. Res. Lett.* **29,** L014683.
24. Ishii, M. & Tromp, J. (1999) *Science* **285,** 1231–1236.
25. Romanowicz, B. (2001) *Geophys. Res. Lett.* **28,** 1107–1110.
26. Forte, A. M., Woodward, R. L. & Dziewonski, A. M. (1994) *J. Geophys. Res.* **99,** 21857–21878.
27. Masters, G. & Gubbins, D. (2003) *Phys. Earth Planet. Int.* **140,** 159–167.
28. Garnero, E., Maupin, V., Lay, T. & Fouch, M. J. (2004) *Science* **306,** 259–261.
29. Kendall, J.-M. & Silver, P. G. (1998) in *Core-Mantle Boundary Region*, Geodynamics Series, eds. Gurnis, M., Wysession, M. E., Knittle, E. & Buffet, B. (Am. Geophys. Union, Washington, DC), Vol. 28, pp. 97–118.
30. McNamara, A. K., van Keken, P. E. & Karato, S. (2002) *Nature* **416,** 310–314.
31. Karki, B. B., Wentzcovitch, R. M., de Gironcoli, S. & Baroni, S. (1999) *Science* **286,** 1705–1707.
32. Wentzcovitch, R. M., Karki, B. B., Karato, S. & Da Silva, C. R. S. (1998) *Earth Planet. Sci. Lett.* **164,** 371–378.
33. Yamazaki, D. & Karato, S. (2002) *Earth Planet. Sci. Lett.* **131,** 251–267.
34. Stixrude, L. (1998) in *Core-Mantle Boundary Region*, Geodynamics Series, eds. Gurnis, M., Wysession, M. E., Knittle, E. & Buffet, B. (Am. Geophys. Union, Washington, DC), Vol. 28, pp. 83–96.
35. Brown, J. M. & Shankland, T. J. (1981) *Geophys. J. R. Astron. Soc.* **66,** 579–596.
36. Tsuchiya, J., Tsuchiya, T. & Wentzcovitch, R. M. (2005) *J. Geophys. Res.* **110,** B02204.
37. Oganov, R., Brodholt, J. & Price, G. D. (2005) *Nature* **411,** 934–937.

Supporting Methods

The techniques used here and the details of this calculation are similar to those used in previous high *P*, *T* calculations of the *Pbmn*-perovskite (1) and *Cmcm* postperovskite phase (2, 3). Computations were performed by using the local density approximation (LDA) (4, 5) and the generalized gradient approximation (6). Pseudopotentials for oxygen and silicon were generated by the method of Troullier–Martins (7). The cut-off radii are (*i*) for oxygen in the configuration $2s^2$ $2p^4$, r(2s) = r(2p) = 1.45 arbitrary units (a.u.), with p locality and (*ii*) for silicon in the configuration $3d^2$ $3p^4$ $3d^0$, r(3s) = r(3p) = r(3d) = 1.47 a.u., with d locality. The method of von Barth–Car (U. von Barth & R. Car, unpublished data) was used for magnesium. Five configurations, $3s^2$ $3p^0$, $3s^1$ $3p^1$, $3s^1$ $3p^{0.5}$ $3d^{0.5}$, $3s^1$ $3p^{0.5}$, and $3s^1$ $3d^1$ with decreasing weights 1.5, 0.6, 0.3, 0.3, and 0.2, respectively were used. Cut-off radii were r(3s) = r(3p) = r(3d) = 2.5 a.u. with d nonlocality. The plane wave energy cutoff was 70 Ry. Brillouin zone sampling for electronic states (phonons) was carried out on 6 (14) and 2 (18) special *k*-points (*q*-points) for the postperovskite and perovskite phases, respectively. Phonon frequencies were obtained by using density functional perturbation theory (8). Structural optimizations were performed by using variable cell shape molecular dynamics (9). Thermodynamic properties were determined by using the quasiharmonic approximation (10).

Our approach to high *P*, *T* elasticity is the same one used previously to calculate the thermoelastic properties of $MgSiO_3$ perovskite (1). It exploits the volume and strain dependence of the vibrational frequencies to determine the thermal contribution to the free energy within the quasiharmonic approximation (QHA). Isothermal elastic constants were obtained as $c_{ij}^T(P,T) = \left[\frac{\partial^2 G(P,T)}{\partial \varepsilon_i \partial \varepsilon_j}\right]_T$, and converted to adiabatic as

$$c_{ij}^S(P,T) = c_{ij}^T(P,T) + \frac{VT}{C_V}\left[\frac{\partial S(P,T)}{\partial \varepsilon_i}\right]_T \left[\frac{\partial S(P,T)}{\partial \varepsilon_j}\right]_T$$

, where *G*, ε_i, *V*, C_V, and *S* are Gibbs free energy, strain, constant volume specific heat, and entropy, respectively. At least 15 strained configurations at each *P*, *T* were required. The magnitude of applied strains was 0.01, as in refs. 1 and 3. The vibrational density of states of postperovskite was sampled at 39, 47, and 60 points throughout the irreducible Brillouin zones of the orthorhombic (ε_1, ε_2, ε_3 deformations) and monoclinic (ε_4, ε_5, and ε_6 deformations) geometries, respectively.

1. Wentzcovitch, R. M., Karki, B. B., Cococcioni, M. & de Gironcoli, S. (2004) *Phys. Rev. Lett.* **92,** 018501.

2. Tsuchiya, T., Tsuchiya, J., Umemoto, K. & Wentzcovitch, R. M. (2004) *Earth Planet. Sci. Lett.* **224,** 241–248.

3. Tsuchiya, T., Tsuchiya, J., Umemoto, K. & Wentzcovitch, R. M. (2004) *Geophys. Res. Lett.* **31,** L14603.

4. Ceperley, D. & Alder, B. (1980) *Phys. Rev. Lett.* **45,** 566–569.

5. Perdew, J. & Zunger, A. (1981) *Phys. Rev. B Condens. Matter* **23,** 5048–5079.

6. Perdew, J. P., Burke, K. & Ernzerhof, M. (1996) *Phys. Rev. Lett.* **77,** 3865–3868.

7. Troullier, N. & Martins, J. L. (1991) *Phys. Rev. B Condens. Matter* **43,** 1993–2006.

8. Giannozzi, P., de Gironcoli, S., Pavone, P. & Baroni, S. (1991) *Phys. Rev. B Condens. Matter* **43,** 7231–7242.

9. Wentzcovitch, R. M., Martins, J. L. & Price, G. D. (1993) *Phys. Rev. Lett.* **70,** 3947–3950.

10. Wallace, D. (1972) *Thermodynamics of Crystals* (Wiley, New York).

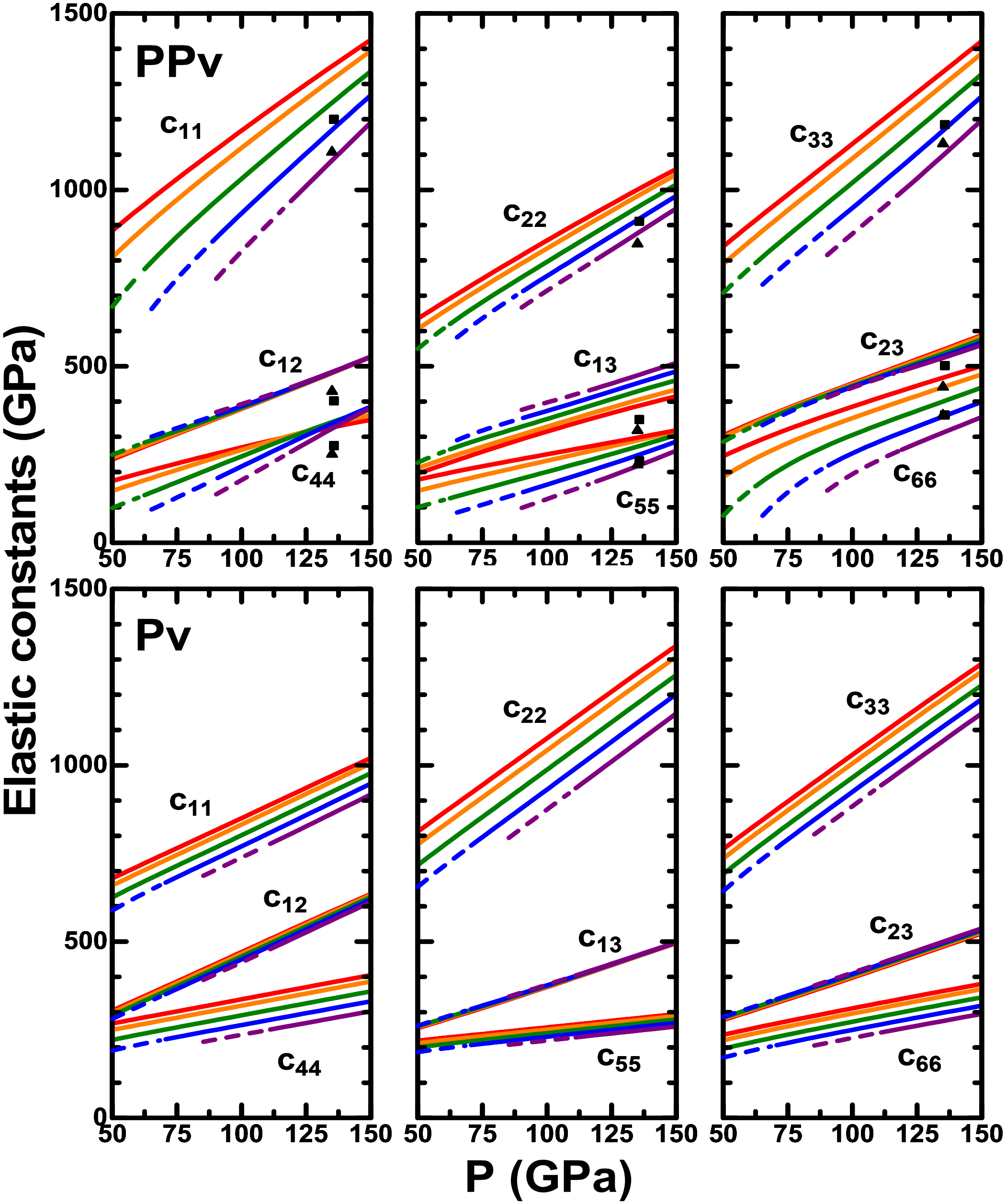
PPv
Pv
c11
c12
c44
c22
c13
c55
c33
c23
c66
Elastic constants (GPa)
P (GPa)
0
500
1000
1500
50
75
100
125
150